F. Berto et alii, Frattura ed Integrità Strutturale, 37 (2017) 69-79; DOI: 10.3221/IGF-ESIS.37.10

Focussed on Multiaxial Fatigue and Fracture

Local strain energy density to assess the multiaxial fatigue strength of titanium alloys

Filippo Berto
University of Padova, Department of Management and Engineering, Vicenza (Italy)
NTNU, Department of Engineering Design and Materials, Trondheim, (Norway)
berto@gest.unipd.it

Alberto Campagnolo
University of Padova, Department of Industrial Engineering, Padova (Italy)
alberto.campagnolo@unipd.it

Torgeir Welo
NTNU, Department of Engineering Design and Materials, Trondheim, (Norway)
torgeir.welo@ntnu.no

ABSTRACT. The present paper investigates the multiaxial fatigue strength of sharp V-notched components made of titanium grade 5 alloy (Ti-6Al-4V). Axisymmetric notched specimens have been tested under combined tension and torsion fatigue loadings, both proportional and non-proportional, taking into account different nominal load ratios (R = -1 and 0). All tested samples have a notch root radius about equal to 0.1 mm, a notch depth of 6 mm and an opening angle of 90 degrees. The fatigue results obtained by applying multiaxial loadings are discussed together with those related to pure tension and pure torsion experimental fatigue tests, carried out on both smooth and notched specimens at load ratios R ranging between -3 and 0.5.
Altogether, more than 250 fatigue results (19 S-N curves) are examined, first on the basis of nominal stress amplitudes referred to the net area and secondly by means of the strain energy density averaged over a control volume embracing the V-notch tip. The effect of the loading mode on the control volume size has been analysed, highlighting a wide difference in the notch sensitivity of the considered material under tension and torsion loadings. Accordingly, the control radius of the considered titanium alloy (Ti-6Al-4V) is found to be strongly affected by the loading mode.

KEYWORDS. Ti-6Al-4V; Multiaxial fatigue; V-notch; Control volume; Strain Energy Density.

INTRODUCTION

For a wide comparison between different approaches adopted to the multiaxial fatigue strength assessment of metallic materials, the reader is referred to a recent review [1] and a report [2], which are based on a large bulk of experimental data obtained from notched specimens. A fundamental role is occupied by critical plane approaches

[3,4] and by some important variants [5-7].
In this context, approaches based on energy calculations find significant applications [8]. A multiaxial fatigue approach based on a frequency-domain formulation of a stress invariant, the so-called "Projection by Projection" (PbP) criterion has been reported in the recent literature [9]. The critical plane-based Carpinteri-Spagnoli approach has recently been extended to a frequency-domain formulation [10]. An energy-based parameter has been adopted to assess the fatigue strength under uniaxial fatigue loadings first by Jasper [11] in 1923. Then, Ellyin suggested a criterion based on the combination of plastic and elastic strain energy [12-13], to deal with multiaxial fatigue loadings. A wide review of energy-based criteria for multiaxial fatigue strength assessment has been reported in [14]. Moreover, the problems relevant to multiaxial fatigue have been investigated both theoretically and experimentally by several researchers [15-22].
This contribution is aimed to analyse the fatigue strength of severely notched titanium grade 5 alloy under multiaxial loadings. The considered titanium alloy (Ti-6Al-4V) is widely employed in advanced military, civil aerospace and naval applications. The in-service conditions of titanium structural components are usually characterized by a complex stress state coupled with an aggressive environment. The titanium grade 5 alloy has high static and fatigue properties, a very good strength-to-mass ratio and an excellent wear resistance. The uniaxial fatigue strength of un-notched and notched titanium components has been extensively analysed in the literature. However, a complete set of experimental data relevant to sharp V-notched specimens made of Ti-6Al-4V and subjected to torsion and combined tension and torsion loadings, both proportional and non-proportional, is not available in the literature. To fill this lack, a complete set of experimental data from sharp V-notched components made of titanium grade 5 alloy (Ti-6Al-4V) under multiaxial fatigue loading is provided here.
Experimental fatigue tests under combined tension and torsion loadings have been carried out on circumferentially V-notched specimens, with two nominal load ratios, namely R = -1 and R = 0. The fatigue results obtained by applying multiaxial loadings are compared with those related to pure tension and pure torsion experimental fatigue tests, carried out on both smooth and notched specimens at load ratios R ranging between -3 and 0.5.
All in all, more than 250 fatigue data (19 Wöhler curves) are examined in terms of nominal stress amplitudes referred to the net area. Then, the experimental fatigue strength data have been reanalysed in terms of the strain energy density (SED) averaged over a control volume embracing the notch tip [23-31]. The effect of the loading mode on the control volume size has been analysed, highlighting the need to use a different control radius under tension and torsion loading, due to a wide difference in the notch sensitivity of the considered material under tension and torsion loadings. The expressions for calculating the control radii, thought of as material properties, have been derived by imposing the constancy of the averaged SED relevant to un-notched and notched specimens, which depend on the critical notch stress intensity factors (NSIFs) and the control radius, in correspondence of $2 \cdot 10^6$ cycles.
The unifying capacity of the averaged SED criterion is highlighted, indeed the synthesis on the basis of the local SED enables to obtain a quite narrow scatter-band, which is characterised by an equivalent stress-based scatter index T_σ equal to 1.58, taking into account all fatigue strength data relevant to notched and un-notched components subjected to pure tension, pure torsion and multiaxial loadings, independently of the nominal load ratio and the phase angle.
Some of the results reported in the present manuscript have been previously presented and extensively discussed in [31].

MATERIAL AND GEOMETRY OF THE SPECIMENS

The material taken into consideration in the present contribution is a titanium grade 5 alloy, also known as Ti-6Al-4V. The geometries of smooth and sharply notched specimens are reported in Fig. 1, along with some details of the V-notch tip. The hourglass smooth specimens, shown in Fig. 1a, are characterized by a 12-mm-diameter of the net transverse area and by a wide connecting radius between the net and gross sections, ρ = 100 mm, so that any stress concentration is avoided.
The cylindrically V-notched samples, shown in Fig. 1b, are characterized, instead, by a notch depth d equal to 6 mm and a notch angle of 90 degrees, while the notch tip radius, ρ, is about equal to 0.1 mm. In particular, the notch root radius has been experimentally measured through an optical microscope and the dedicated software LAS (Leica Application Suite) and a mean value of 0.09 mm with a very reduced scatter has been obtained. The precision ensured by the adopted method is about ± 5% of the measured quantity. The typical V-notch profile characterised by two rectilinear flanks tangent to the notch tip radius is reported in Fig. 1b, for an example of the tested samples.
To remove any scratches or processing marks on the surface, all specimens were polished before the fatigue test.

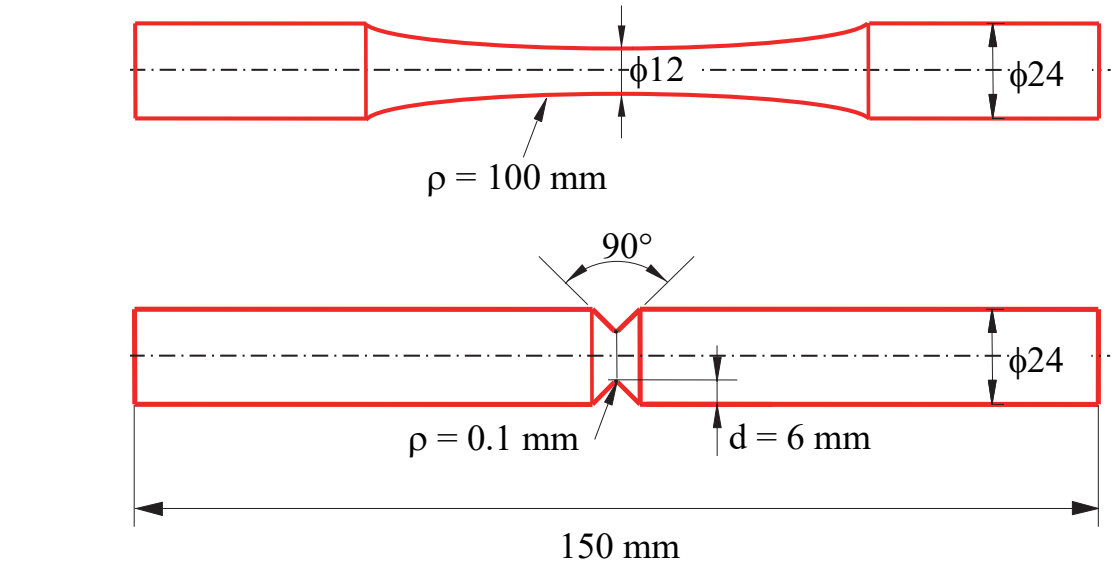

(a)

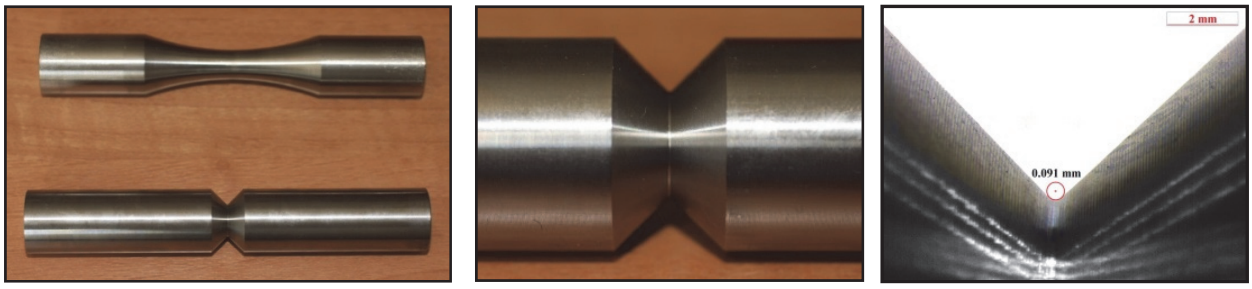

(b)

Figure 1. (a) Geometries of smooth and sharply notched specimens and (b) examples of tested specimens.

EXPERIMENTAL RESULTS FROM FATIGUE TESTS

The experimental fatigue tests have been carried out by means of a MTS 809 servo-hydraulic bi-axial testing device (± 100 kN, ± 1100 Nm, ± 75mm/± 55°) under load control conditions. In particular, a MTS load cell with ± 0.5 % error at full scale has been employed to evaluate the nominally applied loads. A test frequency between 10 and 15 Hz has been adopted as a function of the applied load level.
All in all, 19 different fatigue test series are performed, according to the parameters reported below:

- Four series of fatigue tests on smooth and sharply notched samples subjected to pure tension and pure torsion fatigue loadings, with a nominal load ratio R = -1;
- Four series of fatigue tests on smooth and sharply notched samples subjected to pure torsion fatigue loading, with nominal load ratios R = 0 and 0.5;
- Three series of fatigue tests on smooth samples subjected to pure torsion fatigue loading, with nominal load ratios R = 0.25, -2 and -3;
- Four series of fatigue tests on sharply notched samples subjected to combined tension and torsion loadings, at a constant biaxiality ratio λ = 0.6. Two load ratios, R = 0 and R = -1 (referred separately to the normal and shear

stress components), and two phase angles, $\Phi = 0°$ (proportional loadings) and $\Phi = 90°$ (non-proportional loadings), are employed;

- Four series of fatigue tests on sharply notched samples subjected to combined tension and torsion loading, at a constant biaxiality ratio $\lambda = 2.0$. Also in this case, two load ratios, R = 0 and R = -1, and two phase angles, $\Phi = 0°$ (proportional loadings) and $\Phi = 90°$ (non-proportional loadings), are adopted.

The statistical re-analyses of the fatigue strength data were carried out by assuming a log-normal distribution. All experimental data relevant to specimens with a fatigue life in the range $10^4 \div 2 \cdot 10^6$ cycles have been considered, while the run-outs have been excluded. In particular, Tab. 1 reports the nominal stress amplitudes for a probability of survival Ps = 50% and a number of cycles $N_A = 2 \cdot 10^6$, the inverse slope k of the Wöhler curves and the scatter-index T, which gives a measure of the width of the scatter band, between the curves with 10% and 90% probabilities of survival (with a confidence level equal to 95%).
Under multiaxial loading, the fatigue life results to be reduce if compared to the uniaxial loading case, with reference to the same normal stress amplitude, however the reduction is quite limited for the biaxiality ratios considered herein ($\lambda = 0.6$ and 2.0). Stronger is the multiaxial fatigue strength reduction tied to the effect of the load ratio R. On the other hand, the phase angle effect is weak for R = -1, being the mean values of the normal stress amplitudes about the same at $2 \cdot 10^6$ cycles. While, it is higher for R = 0, being the out-of-phase loading slightly beneficial with respect to in-phase loading at high-cycle fatigue regime, whereas the fatigue strength is almost the same at low-cycle regime. The sensitivity of the considered titanium alloy to the phase angle effect results to be quite limited, being lower than +15 percent for the R = 0 case and negligible for the R = -1 case.
The fracture surfaces relevant to the specimens subjected to multiaxial loadings were examined. The phase angle seems to affect the fracture surface morphology. Indeed, some signs of micro abrasions could be seen on all fracture surfaces and the extent to which the rubbing occurred depends on phase angle. In general, a limited but distinguishable quantity of debris and powder has been emanated from the notch tip, when a visible fatigue crack started to propagate.

SYNTHESIS BASED ON THE AVERAGED STRAIN ENERGY DENSITY

With regard to un-notched specimens, all fatigue results have been summarised here in terms of the averaged SED, which can be expressed, under linear elastic conditions, by means of Beltrami's expression. Accordingly, in the case of pure tension loading, the local strain energy density is given by:

$$\Delta\overline{W} = \frac{\Delta\sigma_{nom}^2}{2E} \tag{1}$$

while in the case of pure torsion loading it is given by:

$$\Delta\overline{W} = (1+\nu)\frac{\Delta\tau_{nom}^2}{E} \tag{2}$$

In previous expressions, $\Delta\sigma_{nom}$ and $\Delta\tau_{nom}$ are the nominal stress ranges tied to tension and torsion loadings, respectively. For the considered titanium alloy, the Young's modulus E results to be 110 GPa, while the Poisson's ratio ν is 0.3.
Then, also the fatigue strength results relevant to notched samples have been reanalysed here in terms of the averaged SED, however, in this case the strain energy calculation is based on the local stress and strain state in a control volume embracing the V-notch tip. Since the notch root radius is reduced (ρ less than 0.1 mm), the Mode I and Mode III NSIFs, K_1 and K_3, can be adopted to summarised the experimental data relevant to notched samples in terms of the local strain energy density. These parameters, which describe the local stress fields, have been evaluated from linear elastic FE analyses taking into consideration a sharp V-notch with tip radius ρ equal to 0 (see Fig. 2). Let us consider a cylindrical coordinate system (r, θ, z) with origin at the notch tip, where r is the radial coordinate, θ is the angle between a generic point and the notch bisector line, while z is the longitudinal axis of the specimen. In particular, with reference to this coordinate system (see Fig. 2), the Mode 1 and Mode 3 NSIFs can be defined by means of the following expressions:

$$K_1 = \sqrt{2\pi}\lim_{r\to 0^+} r^{1-\lambda_1}\sigma_{\theta\theta}(r,\theta=0) \quad (3)$$

$$K_3 = \sqrt{2\pi}\lim_{r\to 0^+} r^{1-\lambda_3}\tau_{\theta z}(r,\theta=0) \quad (4)$$

Table 1. Experimental results from fatigue tests. Mean values, P_s = 50%. Stresses referred to the net area.

Series	Type of load	Number of specimens		k	T_σ T_τ	σ_a or τ_a $2 \cdot 10^6$
1	Tension R = -1	12	σ	9.25	1.120	475.74
2	Torsion R = -1	16	τ	22.13	1.205	388.25
3	Torsion R = 0	9	τ	15.03	1.322	287.22
4	Tension R = -1, V-notch 2α = 90°	15	σ	6.26	1.133	100.89
5	Torsion R = -1, V-notch 2α = 90°	9	τ	14.59	1.229	289.31
6	Torsion R = 0, V-notch 2α = 90°	11	τ	13.82	1.159	247.16
7	Torsion R = 0.5, V-notch 2α = 90°	7	τ	19.91	1.080	169.89
8	Multiaxial R = -1, Φ = 0°, λ= 0.6, V-notch 2α = 90°	13	σ τ	6.82	1.197	93.89 56.39
9	Multiaxial R = -1, Φ = 90°, λ = 0.6, V-notch 2α = 90°	10	σ τ	7.84	1.124	96.11 57.67
10	Multiaxial R = 0, Φ = 0°, λ = 0.6, V-notch 2α = 90°	12	σ τ	8.09	1.159	67.74 40.64
11	Multiaxial R = 0, Φ = 90°, λ = 0.6, V-notch 2α = 90°	12	σ τ	10.43	1.158	79.65 47.79
12	Torsion R = 0.5	12	τ	21.19	1.134	180.73
13	Torsion R = 0.25	8	τ	25.67	1.078	268.12
14	Torsion R = -3	7	τ	16.25	1.178	357.55
15	Torsion R = -2	8	τ	21.32	1.042	409.01
16	Multiaxial R = -1, Φ = 0°, λ = 2, V-notch 2α = 90°	26	σ τ	7.61	1.118	75.94 37.97
17	Multiaxial R = -1, Φ = 90°, λ = 2, V-notch 2α = 90°	22	σ τ	7.59	1.114	84.70 42.35
18	Multiaxial R = 0, Φ = 0°, λ = 2, V-notch 2α = 90°	21	σ τ	8.01	1.125	59.75 29.88
19	Multiaxial R = 0, Φ = 90°, λ = 2, V-notch 2α = 90°	21	σ τ	9.40	1.089	65.97 32.99

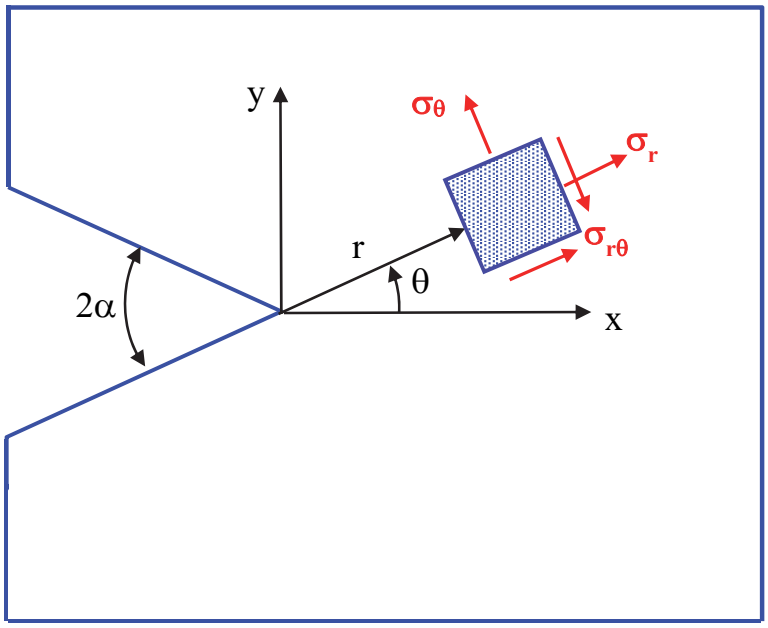

Figure 2. Polar coordinate system for V-shaped notches, with z normal to the plane; Mode I NSIF linked to the stress component σ_θ evaluated along the notch bisector line (θ=0); under mode III the shear stress component $\tau_{z\theta}$ is oriented as σ_θ.

Considering an opening angle of 90 degrees, the eigenvalues λ_1 and λ_3 result to be 0.545 and 0.667, respectively. Moreover, under linear elastic conditions, the NSIFs can be linked to the nominal stress components as follow:

$$\Delta K_1 = k_1 d^{1-\lambda_1} \Delta\sigma_{nom} \quad (5a)$$

$$\Delta K_3 = k_3 d^{1-\lambda_3} \Delta\tau_{nom} \quad (5b)$$

In previous expressions, d represents the notch depth (d = 6.0 mm), while k_1 and k_3 are the non-dimensional factors obtained by means of proper FE analyses. They represent the shape factors, similarly to the expressions of stress intensity factors in Linear Elastic Fracture Mechanics. The quadrilateral eight-node harmonic element PLANE 83 of the Ansys® element library has been adopted in the FE analyses. Taking advantage of the symmetry conditions, only one quarter of the sample geometry has been modelled. According to the FE analyses carried out, k_1 is equal to 1.000, while k_3 equals 1.154.

The trend of the Mode III stress field, normalized with respect to the nominally applied shear stress and evaluated on the notch bisector line, is reported in Fig. 3 as a function of the distance from the notch tip. It can be observed that the stress field is controlled by the first singular term (NSIF) up to a distance from the notch tip about equal to 1.0 mm.

Taking into account the notch depth of the tested samples, namely d = 6 mm, in previous Eqs (5a) and (5b), the following simple expressions can be obtained:

$$\Delta K_1 = 2.260 \cdot \Delta\sigma_{nom} \quad (\text{in MPa} \cdot \text{mm}^{0.445}) \quad (6a)$$

$$\Delta K_3 = 2.096 \cdot \Delta\tau_{nom} \quad (\text{in MPa} \cdot \text{mm}^{0.333}) \quad (6b)$$

By substituting into Eqs. (6a) and (6b) the ranges of the nominal stresses at $N_A = 2 \cdot 10^6$ cycles relevant to notched samples subjected to pure tension and pure torsion loadings at a nominal load ratio R = -1 (see Tab. 1), one can obtain:

$$\Delta K_{1A} = 2.260 \cdot 200 = 452 \text{MPa} \cdot \text{mm}^{0.445} \quad (7a)$$

$$\Delta K_{3A} = 2.096 \cdot 580 = 1216 MPa \cdot mm^{0.333} \quad (7b)$$

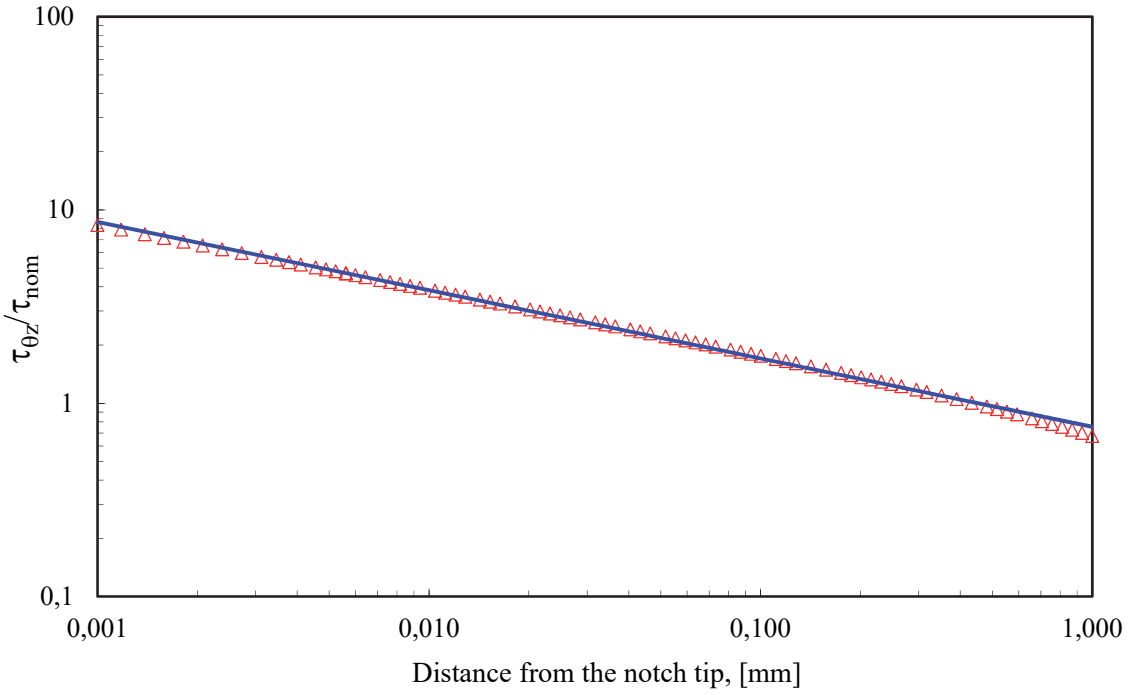

Figure 3. Local shear stress field along the notch bisector line (Mode III loading).

Dealing with a sharp V-notched component subjected to combined tension and torsion loadings under linear elastic conditions, the strain energy density averaged over a control volume surrounding the notch tip can be evaluated from the following closed-form expression:

$$\Delta\overline{W} = \frac{1}{E}\left[e_1 \cdot \frac{\Delta K_1^2}{R_1^{2(1-\lambda_1)}} + e_3 \cdot \frac{\Delta K_3^2}{R_3^{2(1-\lambda_3)}} \right] \quad (8)$$

In previous expression, ΔK_1 and ΔK_3 are the Mode I and Mode III NSIF ranges, respectively, R_1 and R_3 represent the control volume sizes related to Mode I and Mode III loadings, respectively, while e_1 and e_3 are known coefficients which take into account the local notch geometry. These parameters are tied to the integrals over the control volume of the angular stress functions and they can be evaluated a-priori by means of closed-form expressions, as a function of the notch opening angle. Being the tested samples characterized by an opening angle 2α of 90 degrees, e_1 and e_3 result to be 0.146 and 0.310, respectively, with reference to a Poisson's ratio $\nu = 0.3$.

Very refined FE meshes must be adopted in the close vicinity of the singularity point to evaluate the NSIFs on the basis of definitions (3) and (4). On the other hand, the local SED results to be insensitive to the mesh refinement. Indeed, it can be accurately calculated also from FE analyses with coarse meshes, since it directly depends on nodal displacements. The most important and useful advantages tied to the use of the averaged strain energy density parameter are analysed and discussed in detail in Ref. [30].

The expressions for calculating the control radii, thought of as material properties, have been derived by imposing the constancy of the averaged SED relevant to un-notched and notched specimens, which depend on the critical notch stress intensity factors (NSIFs) and the control radius, in correspondence of $2 \cdot 10^6$ cycles. By taking into consideration, instead, cracked samples, the critical NSIFs should be substituted by the threshold values of the stress intensity factors. By considering the Mode I and Mode III loading conditions as independent, the control radii R_1 and R_3 (as shown in Fig. 4) can be estimated. In particular, they result to be dependent on the high-cycle fatigue strengths of un-notched specimens,

$\Delta\sigma_{1A}$ = 950 MPa and $\Delta\tau_{3A}$ = 776 MPa, and on the mean values of the NSIFs, ΔK_{1A} and ΔK_{3A}, with reference to a given number of cycles, $N_A = 2 \cdot 10^6$:

$$R_1 = \left(\sqrt{2e_1} \cdot \frac{\Delta K_{1A}}{\Delta \sigma_{1A}} \right)^{\frac{1}{1-\lambda_1}} \tag{9a}$$

$$R_3 = \left(\sqrt{\frac{e_3}{1+\nu}} \cdot \frac{\Delta K_{3A}}{\Delta \tau_{3A}} \right)^{\frac{1}{1-\lambda_3}} \tag{9b}$$

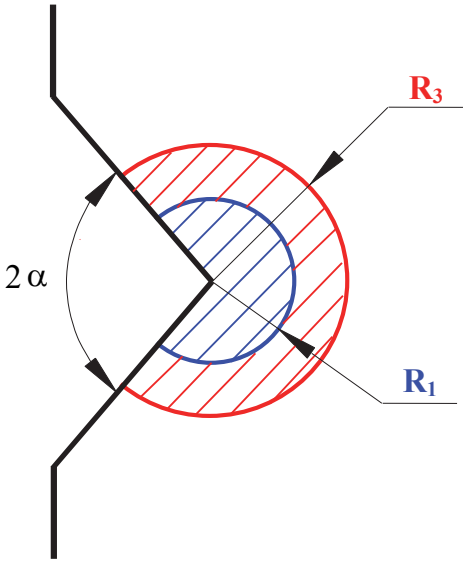

Figure 4. Control volumes for V-shaped notches under tension and torsion loadings.

On the basis of Eqs. (9a) and (9b), the control radii result to be R_1 = 0.051 mm and R_3 = 0.837 mm, respectively. Accordingly, the control radius R_1 has been adopted to compute the averaged strain energy contribution tied to tension loading, whereas the control radius R_3 has been employed to evaluate the averaged SED contribution due to torsion loading. It should be noted that the control radius R_3 is highly affected by the presence of larger plasticity under torsion loading as compared to tension loading, and by friction and rubbing between the crack surfaces, as previously discussed also for different materials [23,30]. Under these conditions, the averaged SED is called also 'apparent linear elastic SED' to highlight that the strain energy density calculation over two different control volumes (under tension and torsion, respectively, as determined from experimental data) allows us to overcome the problem tied to shielding mechanisms, keeping a linear elastic criterion.

To summarise in the same scatter band experimental results obtained by adopting different nominal load ratios R, a coefficient c_w, defined on the basis of simple algebraic considerations (reported in detail in Ref. [24, 31]), must be introduced. The coefficient c_w results to be dependent on the nominal load ratio R according to the following expression:

$$c_W = \begin{cases} \dfrac{1+R^2}{(1-R)^2} & \text{for} \quad -\infty \le R \le 0 \\ 1 & \text{for} \quad R = 0 \\ \dfrac{1-R^2}{(1-R)^2} & \text{for} \quad 0 \le R \le 1 \end{cases} \tag{10}$$

The parameter c_w equals 1.0 in the case R = 0, while it results equal to 0.5 for R = -1. By adopting the coefficient c_w, the closed-form expressions to evaluate the averaged SED, related to smooth samples (Eqs. (1, 2)) and to components weakened by sharp notches (Eq. (8)), become as follow:

$$SED = \begin{cases} c_W \cdot \dfrac{\Delta\sigma_{nom}^2}{2E} & \text{un-notched specimens pure tension} \\ c_W \cdot (1+\nu)\dfrac{\Delta\tau_{nom}^2}{E} & \text{un-notched specimens pure torsion} \\ \dfrac{c_W}{E}\left[e_1 \cdot \dfrac{\Delta K_1^2}{R_1^{2(1-\lambda_1)}} + e_3 \cdot \dfrac{\Delta K_3^2}{R_3^{2(1-\lambda_3)}}\right] & \text{V-notched specimens multiaxial loading} \end{cases} \quad (11)$$

Fig. 5 reports the synthesis of all experimental fatigue results analysed in the present contribution by means of the averaged SED. The control radius R_1 = 0.051 mm has been adopted to evaluate the SED contribution due to tension loading, while the control radius R_3 = 0.837 mm has been employed for the SED contribution due to torsion loading. All fatigue strength results relevant to smooth and notched samples under pure tension, pure torsion and multiaxial loading conditions are included in the obtained scatter band, independently of the nominal load ratio and of the phase angle. The design scatter band is characterized by an inverse slope k of 5.90, by an energy-based scatter index T_W = 2.50 and by a SED value at $N_A = 2 \cdot 10^6$ cycles equal to 3.08 MJ/m^3. However, the equivalent stress-based scatter index, that is $T_\sigma = (T_W)^{0.5}$, equals 1.58, which is very similar to that of the Haibach scatter band (T_σ = 1.50). It should be noted that an extensive review of the considered experimental results will be carried out in the special issue dedicated to the 11th International Conference on Multiaxial Fatigue and Fracture (ICMFF11) [32].

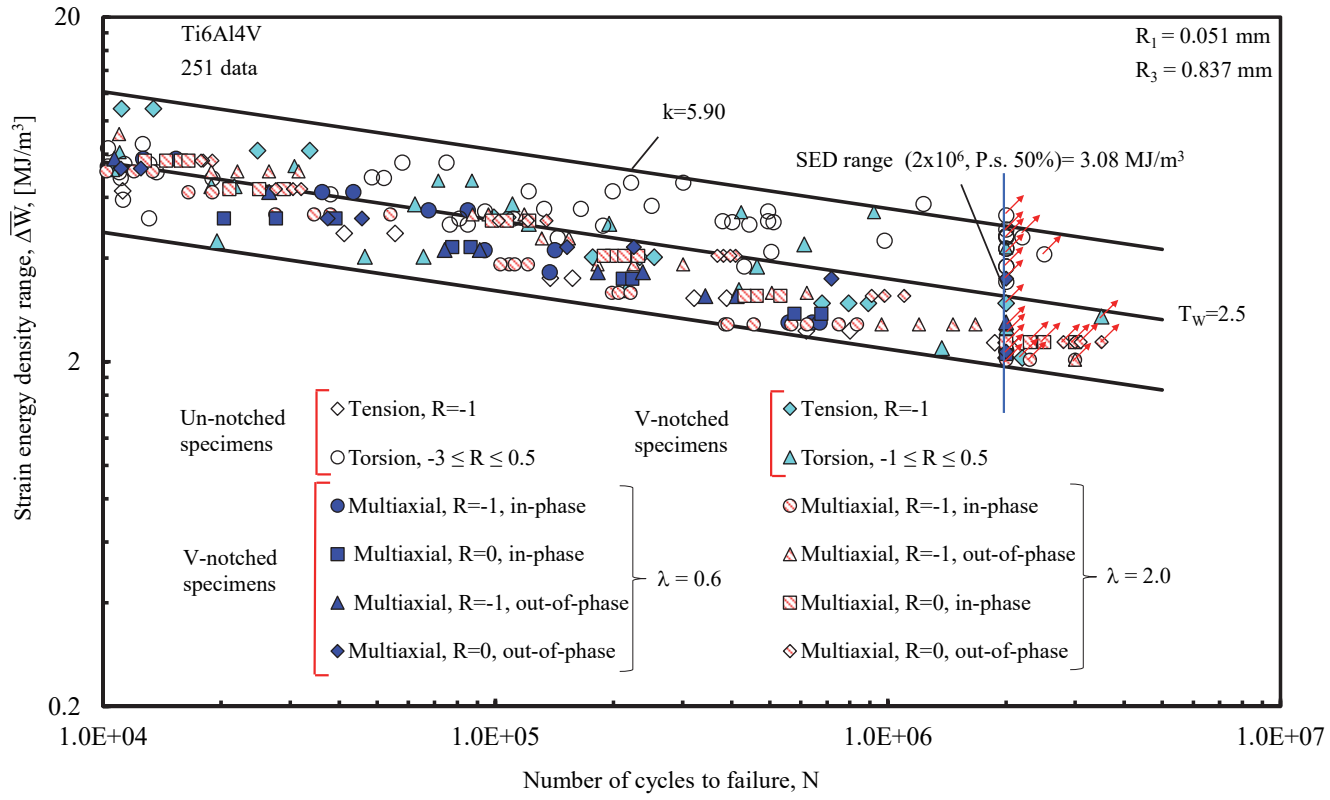

Figure 5. Local SED-based synthesis of experimental fatigue results relevant to smooth and sharply notched specimens. Almost 250 fatigue data are summarised in the scatter band.

CONCLUSIONS

A large bulk of experimental fatigue results relevant to axisymmetric notched samples subjected to multiaxial loadings, both proportional and non-proportional, have been re-analysed and compared with the fatigue strength data relevant to smooth and notched samples subjected to pure tension and pure torsion loadings. All specimens were made of titanium grade 5 alloy (Ti-6Al-4V).

Altogether, more than 250 fatigue results, corresponding to 19 S-N curves, have been analysed in this contribution. First, the experimental results obtained from uniaxial and multiaxial fatigue tests have been examined on the basis of nominal stress amplitudes. Then, they have been re-analysed by means of the linear elastic strain energy density (SED) averaged over a control volume surrounding the notch root. The effect of the loading mode on the control volume size has been analysed in detail, showing that different control radii must be adopted under tension and torsion loading conditions, dealing with notched components made of Ti-6Al-4V titanium alloy.

The averaged SED-based synthesis enables to obtain a quite narrow scatter band, characterized by an energy-based scatter index of 2.50. In particular, the fatigue design scatter band was derived by taking into account all experimental results relevant to smooth and notched samples under pure tension, pure torsion and multiaxial loading conditions, regardless the nominal load ratio and the phase angle.

REFERENCES

[1] Fatemi, A., Shamsaei, N., Multiaxial fatigue: An overview and some approximation models for life estimation, Int. J. Fatigue, 33 (2011) 948-958.

[2] Nieslony, A., Sonsino, C.M., Comparison of some selected multiaxial fatigue assessment criteria, L.B.F. Report, No. FB-234 (2008).

[3] Fatemi, A., Socie, D.F., A critical plane approach to multiaxial fatigue damage including out-of-phase loading, Fatigue Fract. Eng. Mater. Struct., 11 (1988) 149-165.

[4] Fatemi, A., Kurath, P. P., Multiaxial fatigue life prediction under the influence of mean stresses, ASME J. Eng. Mater. Techn., 110 (1988) 380-388.

[5] Łagoda, T., Macha, E., Bedkowski, W., A critical plane approach based on energy concepts: application to biaxial random tension-compression high-cycle fatigue regime, Int. J. Fatigue, 21 (1999) 431-443.

[6] Carpinteri, A., Spagnoli, A., Multiaxial high-cycle fatigue criterion for hard metals, Int. J. Fatigue, 23 (2001) 135-145.

[7] Carpinteri, A., Spagnoli, A., Vantadori, S., Bagni, C., Structural integrity assessment of metallic components under multiaxial fatigue: The C-S criterion and its evolution, Fatigue Fract. Eng. Mater., 36 (2013) 870-883.

[8] Ye, D., Hertel, O., Vormwald, M., A unified expression of elastic–plastic notch stress–strain calculation in bodies subjected to multiaxial cyclic loading, Int. J. Solids Struct., 45 (2008) 6177-6189.

[9] Cristofori, A., Benasciutti, D., Tovo, R., A stress invariant based spectral method to estimate fatigue life under multiaxial random loading, Int. J. Fatigue, 33 (2011) 887–899.

[10] Carpinteri, A., Spagnoli, A., Vantadori, S., Reformulation in the frequency domain of a critical plane-based multiaxial fatigue criterion, Int. J. Fatigue, 67 (2014) 55-61.

[11] Jasper, T.M., The value of the energy relation in the testing of ferrous metals at varying ranges and at intermediate and high temperature, Philos. Mag., 46 (1923) 609–627.

[12] Ellyin, F., Cyclic strain energy density as a criterion for multiaxial fatigue failure, Brown, Miller, editors. Biaxial and Multiaxial Fatigue, London: EGF Publication, (1989) 571–83.

[13] Ellyin, F., Fatigue damage, crack growth and life prediction, Edmonton: Chapman and Hall (1997).

[14] Macha, E., Sonsino, C. M., Energy criteria of multiaxial fatigue failure, Fatigue Fract. Engng. Mater. Struct., 22 (1999) 1053–1070.

[15] Pook, L.P., Sharples, J.K., The mode III fatigue crack growth threshold for mild steel, Int. J. Fract., 15 (1979) R223-R226.

[16] Pook, L.P., The fatigue crack direction and threshold behaviour of mild steel under mixed mode I and III loading, Int. J. Fatigue, 7 (1985) 21-30.

[17] Tong, J., Yates, J.R., Brown, M.W., Some aspects of fatigue thresholds under mode III and mixed mode and I loadings, Int. J. Fatigue, 18 (1986) 279-285.

[18] Yu, H.C., Tanaka, K., Akiniwa, Y., Estimation of torsional fatigue strength of medium carbon steel bars with circumferential crack by the cyclic resistance-curve method, Fatigue Fract. Eng. Mater. 21 (1998) 1067-1076.
[19] Tanaka, K., Akiniwa, Y., Yu, H., The propagation of a circumferential fatigue crack in medium-carbon steel bars under combined torsional and axial loadings, In: Mixed-Mode Crack Behaviour, ASTM 1359 (eds Miller, K.J., McDowell, D.L.), West Conshohocked, PA, (1999) 295-311.
[20] Pippan, R., Zelger, C., Gach, E., Bichler, C., Weinhandl, H., On the mechanism of fatigue crack propagation in ductile metallic materials, Fatigue Fract. Engng. Mat. Struct. 34 (2011) 1-16.
[21] Christopher, C.J., James, M.N., Patterson, E.A., Tee, K.F., Towards a new model of crack tip stress fields, Int. J. Fracture, 148 (2007) 361–371.
[22] Christopher, C.J., James, M.N., Patterson, E.A., Tee, K.F., A quantitative evaluation of fatigue crack shielding forces using photoelasticity, Eng. Fract. Mech. 75 (2008) 4190-4199.
[23] Berto, F., Lazzarin, P., Yates, J., Multiaxial fatigue of V-notched steel specimens: a non-conventional application of the local energy method, Fatigue Fract. Engng. Mater. Struct. 34 (2011) 921–943.
[24] Lazzarin, P., Sonsino, C.M., Zambardi, R., A notch stress intensity approach to assess the multiaxial fatigue strength of welded tube-to-flange joints subjected to combined loadings, Fatigue Fract. Engng. Mater. Struct. 27 (2004) 127-140.
[25] Berto, F., Lazzarin, P., Fatigue strength of structural components under multi-axial loading in terms of local energy density averaged on a control volume, Int. J. Fatigue, 33 (2011) 1055-1065.
[26] Berto, F. , Lazzarin, P., Marangon, C., Fatigue strength of notched specimens made of 40CrMoV13.9 under multiaxial loading, Mater. Des., 54 (2014) 57-66.
[27] Berto, F., Lazzarin, P., Tovo, R., Multiaxial fatigue strength of severely notched cast iron specimens, Int. J. Fatigue, 67 (2014) 15-27.
[28] Berto, F., Campagnolo, A., Chebat, F., Cincera, M., Santini, M., Fatigue strength of steel rollers with failure occurring at the weld root based on the local strain energy values: modelling and fatigue assessment, Int. J. Fatigue. 82 (2016) 643–657. doi:10.1016/j.ijfatigue.2015.09.023.
[29] Campagnolo, A., Berto, F., Leguillon, D., Fracture assessment of sharp V-notched components under Mode II loading: a comparison among some recent criteria, Theor. Appl. Fract. Mech. (2016) in press. doi:10.1016/j.tafmec.2016.02.001.
[30] Berto, F., Lazzarin, P., Recent developments in brittle and quasi-brittle failure assessment of engineering materials by means of local approaches, Mater. Sci. Eng. R, 75 (2014) 1-48.
[31] Berto, F., Campagnolo, A., Lazzarin, P., Fatigue strength of severely notched specimens made of Ti-6Al-4V under multiaxial loading, Fatigue Fract. Eng. Mater. Struct. 38 (2015) 503-517.
[32] Berto, F., Campagnolo, A., Welo, T., Multiaxial fatigue strength of titanium alloys, Int. J. Fatigue, (to be submitted).